



Using GPR to analyze regeneration success of cork oaks in the Maâmora forest (Morocco)

Aurore de Mahieu^{a,*}, Quentin Ponette^a, Fouad Mounir^b, Sébastien Lambot^a

^a Université Catholique de Louvain, Earth and Life Institute, Croix Du Sud 2 / L7.05.05, 1348, Louvain-la-Neuve, Belgium

^b National Forestry School of Engineers (ENFI), BP: 511, Tabriquet, Salé, Morocco

ARTICLE INFO

Keywords:

Soil moisture map
Textural transition depth
Cork oak
Maâmora

ABSTRACT

Under limited precipitation, coarse-textured soils may strongly limit tree regeneration success and stand productivity, yet their effective impact depends on layer thickness and the nature of the underlying soil material. Within that context, we have evaluated the performance of two ground-penetrating radar (GPR) techniques to assess the short-scale variability in physical soil properties, using the Maâmora forest and cork oak as a case study. A frequency-domain GPR was developed to map the soil surface water content of a 1 ha, 18-year old cork oak stand. In addition, a time-domain GPR was used to detect soil textural transitions in depth between the sand and clay textures of the same cork oak stand. Intensive GPR measurements were made along transects, together with detailed local stand and soil characterization. The volumetric water contents (θ_v) varied between 0.01 m³/m³ and 0.1 m³/m³, which represent available water storage of coarse sands to sandy loams [0.04 m³/m³ - 0.12 m³/m³]. The estimated transition depths detected by the second GPR varied between 1.8 m and 4.0 m deep. Soil water content was found to be a relevant indicator of successful cork oak regeneration as it was strongly related to the dominant heights of the cork oaks. The most successful areas were characterized by higher surface moisture and these higher values were mostly explained by soil texture. Moreover, the layer thickness also influenced cork oak growth. Hence, both radar systems provided useful predictors for the regeneration success of cork oaks. Using GPR for future tree planting would allow foresters to detect the best areas in terms of hydric and edaphic conditions where trees should be installed in order to ensure a successful establishment.

1. Introduction

Arid and semi-arid lands are fragile ecosystems that cover about one-third of the world land area and are characterized by excessive heat and variable precipitation [1]. Forests of arid zone ecosystems provide shade and shelter for many animal species, regulate water flow, prevent soil erosion and mitigate climate change [2]. They also guarantee food security of hundreds of millions of people for the different sources they provide such as food, energy and income [2].

Soils of these regions are mostly dry coarse-textured soils due to the slow chemical weathering caused by the characteristic water deficit [1]. Soil water availability is commonly the main factor limiting tree establishment and subsequent growth, along with climate and soil fertility [3]. In fact, the water retention capacity of soils depends on physical properties such as soil texture, structure and soil depth [1].

Sandy soils, which prevail in these regions, are coarse-textured and hence, retain little water and have no structure. In order to grow, tree species must rely on a minimum soil water reserve during the dry season and it must develop a root system that grows quickly enough to reach deeper soil horizons that could possibly retain water (e.g., clay-enriched horizons) [4]. This is particularly important for tree seedlings, as their survival will be strongly threatened if their roots do not reach a soil depth that holds water during the dry season. Moreover, natural fertility of sandy soils is often low as the organic matter content of the topsoil is minimal leading to nutrient-poor soils [1]. Tree roots must therefore pair with roots from neighboring trees to exchange nutritive substances or pair with fungi and form mycelia to curb this constraint [5].

Therefore, one pre-requisite to ensure plantation success is to properly assess the potential soil water availability, so as to optimize the planting scheme (e.g., soil preparation, vegetation management,

* Corresponding author.

E-mail addresses: aurore.de.mahieu@gmail.com (A. de Mahieu), quentin.ponette@uclouvain.be (Q. Ponette), mounirf@hotmail.com (F. Mounir), sebastien.lambot@uclouvain.be (S. Lambot).

¹ Present and permanent address.

plantation period, tree species selection etc.) [6].

This justifies the interest of testing ground-penetrating radar (GPR) techniques in order to have access to physical soil factors that influence tree growth. GPR is a mature sensing tool that has been widely used to characterize subsurface structures and properties in many applications [7,8].

In this study, two types of ground-penetrating radars were used. A frequency-domain GPR was developed to map the soil surface water content of a 1 ha stand whereas a commercial time-domain GPR was used to detect soil textural transitions in depths between sand and clay textures. The method consists of combining two different kinds of GPR in order to obtain complementary information of soil properties. The time-domain radar with ground-coupled antennas was used for sufficient depth penetration while the frequency-domain radar with an off-ground antenna was used for accurate full-wave inversion.

The overall aim of this research is to test the GPR benefits to develop a method to characterize spatial variability (lateral and vertical) of soil physical properties potentially involved in the successful regeneration of tree species. This requires to first, proceed in a geophysical characterization of the study area using GPR techniques, then linking the geophysical signal with the physical properties of the soil, and finally linking these properties to plant response. Hence, we chose a forest stand of the Maâmora forest (Morocco) for this study. Soils of this forest can be described as dry sandy horizons that lie above sandy-clay layers. Essentially composed of cork oak (*Quercus suber* L.) from the middle of the 20th century, a net regression of 30% has been estimated since then in Maâmora [9]. This is due to problems in regeneration and successive periods of drought throughout the century. Soil surveys down to 2 m deep were performed as well as sieve analyses. Soil moisture mapping was carried out using a frequency-domain GPR developed in the Georadar Research Centre of the Université catholique de Louvain. Time-domain GPR data were analyzed and dendrometric measurements were taken to study the vigor of the cork oaks.

2. Materials and methods

2.1. Study site

The Maâmora forest is located in North-West Morocco, between Rabat-Salé and Kénitra and extends from the Atlantic Ocean up to 70 km inland. It covers a total area of 131 400 ha and consists of about 65 000 ha of cork oaks, while the rest of its area is covered by more productive exotic tree species such as eucalyptus, acacia and maritime pine [10]. Cork oaks are found in southwestern Europe and northwestern Africa. This evergreen species grows on non-calcareous substrates and prefers sandy and slightly structured soils [5]. It is well adapted to warm and dry climates in its central distribution area but in its southern area, like in the Maâmora forest, previous studies have shown that successful regenerations depend on the capacity for the seedlings to reach the water table or clay layer during the first dry summers of growth [4,11]. Seedling survival will be highly hypothetical if roots do not reach a soil depth that holds water during drought [12]. In this case, the growth of a vast and deep root system will allow the species to cope with droughts.

Maâmora forest plays important ecological and socio-economic roles as it provides a recreational area for populations of neighboring agglomerations and is the main source of income for more than 300 000 inhabitants (e.g., cork harvest, firewood, forage production, non-wood products, etc.) [9]. Unfortunately, as the needs of rural population have increased, Maâmora forest is now under pressure [13]. Degradation of the forest not only results from regeneration issues but also from human activity: illegal harvesting of wood, overgrazing, topping and pruning and collection of acorns are some of the reasons that partly explain the regression of the forest this past century. Nowadays, many development and management plans are established with clear objectives of regeneration and protection of cork oak stands. Artificial regeneration is part of these management plans, as natural regeneration

has been proven insufficient to guarantee sustainability [14].

The bioclimate of Maâmora is sub-humid in the western part of the forest but semi-arid in the central and eastern parts [15]. Hence, a decreasing rainfall gradient from West to East is observable. The mean annual temperature in Rabat-Salé is 17.9 °C and the mean total annual rainfall was 530 mm for the period 1982–2012 [16]. The rainy season occurs between November and March. December is the most humid month with 120 mm of cumulative rainfall, while July is the driest month with less than 1 mm [16].

The soils of the Maâmora forest are typically composed of a more or less deep sand layer (0.3 m–6 m) laying above a clay layer also called the “red clay of Maâmora”. This clay is geologically dated from the Villafranchian period and the sand layers originates from a rearrangement by river or wind actions of the Quaternary sand spreading [17]. The first soil layer is made of two types of sand: (i) red siliceous sands, rich in iron oxides with a minor clay fraction and (ii) pink to beige siliceous sands which are more recent than the first ones and do not contain any clay [4]. The red clay of Maâmora that lies under the sandy layer contains a mixture of three clay minerals: kaolinite, illite and montmorillonite.

The study site is located in the so-called B-canton, in the sub-humid part of the climate gradient (mean total annual rainfall of 550 mm), between forest stands VI-6 and VI-7 (Fig. 1). This specific stand was chosen because of its high variability in terms of tree growth and regeneration success. Many cork oaks of this plot have suffered from different kinds of pressures as evidenced by their relatively low heights and circumferences and low survival rates in distinct areas. Moreover, previous studies of this particular stand have also shown that there is variability in the sand and clay layer depths [18]. The stand has a SW to NE orientation: it is about 700 m long and 150 m wide and covers an area of 1.05 ha. The study stand was artificially regenerated in 1999 using acorn seedlings (mean age of cork oaks at sampling: 18 years old), following cleaning and deep ploughing. Three or four acorns were planted in cubic holes of 20–30 cm deep and then were refilled with soil. The distance between two seedlings is 3 m long and each row of trees is also separated by 3 m. During the first year, the plantation was watered twice (10 l/seedling). Until the third year, weeding and harrowing took place, then, in 2007, individualization occurred to select one tree per seedling. Finally, pruning and thinning took place in 2014 [18].

2.2. Geophysical characterization of soils using GPR

2.2.1. Frequency domain radar system for soil moisture mapping

A portable lightweight frequency-domain GPR was set up to determine the soil surface volumetric water content of the study plot. The radar system consists of a handheld vector network analyzer (VNA, Planar R54, Copper Mountain Technologies, Indianapolis, USA) that transmits stepped-frequency continuous waves. The VNA is capable of measuring the reflection coefficient S_{11} from 85 MHz to 5.4 GHz. The radar measurements are controlled using a homemade software based on a micro-computer and a remote smartphone using a local Wi-Fi network. The radar also consists of a horn dipole antenna made of copper. It is used simultaneously as transmitter and receiver (monostatic mode). Its dimensions are 55 cm long and 25 cm high and it weighs about 1 kg. It was self-designed at the Georadar Research Centre (UCLouvain) to adapt its frequency range to the requirements of the project (i.e., relatively low frequencies). The radar system is illustrated in Fig. 2. Preliminary antenna calibration and laboratory tests were accomplished in order to use this new radar system in the Maâmora forest. To calibrate the antenna, i.e., to determine its characteristic transfer functions H_i , H_r , and H_f , we used the far-field model developed by Lambot et al. [19,20]. The measurements were performed at seven different heights over a 3 m × 3 m copper sheet. For each height, 10 to 15 measurements were recorded by the radar and subsequently averaged. Laboratory tests were also carried out on a perfectly dried sand to confirm the proper functioning of the radar system and to define the accurate calibration of the antenna model. Finally, numerical

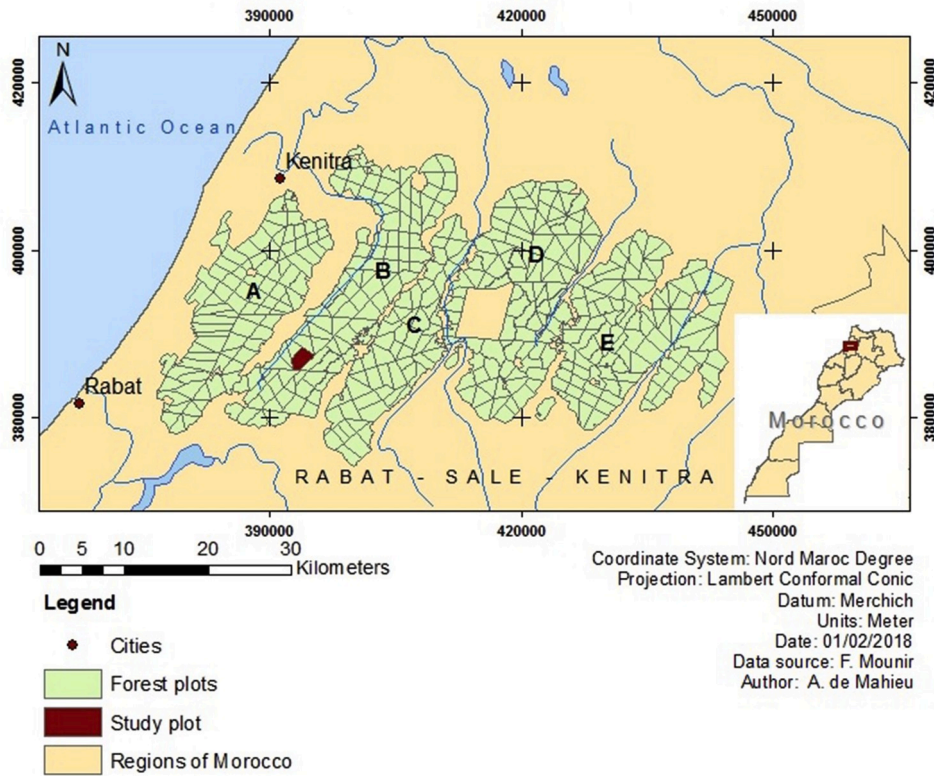


Fig. 1. Geographical location of the Maâmorra forest, subdivided into 5 cantons and into 450 parcels. The study site is indicated in red. (Color should be used). (For interpretation of the references to color in this figure legend, the reader is referred to the Web version of this article.)

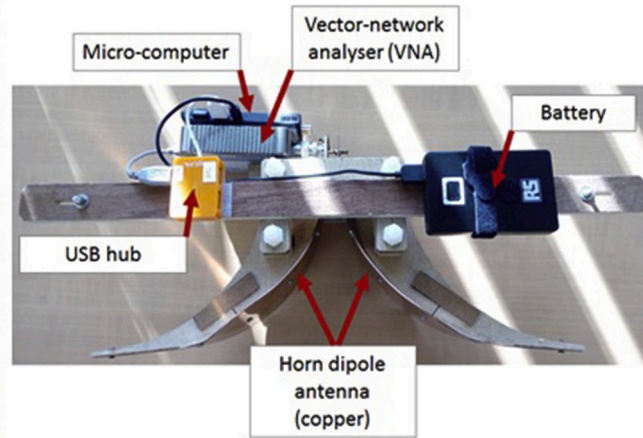


Fig. 2. Portable lightweight frequency-domain radar system composed of a horn dipole antenna made of copper, a VNA, a micro-computer, a USB-hub, a battery and a handle. A lightweight GPS (GlobalSat BU-353S4) is also connected to the Intel Compute Stick for positioning of the radar data. (a) GPR with handle in Maâmorra forest. (b) Close up of the radar system. (Color should be used). (For interpretation of the references to color in this figure legend, the reader is referred to the Web version of this article.)

simulations were performed to test the GPR in similar conditions to those expected in the Maâmorra forest.

• Full-wave GPR data inversion

As explained above, we set up a frequency-domain radar system using a lightweight vector network analyzer (VNA) technology. In that case, the radar signal consists of the frequency-dependent complex ratio $S_{11}(\omega)$, between the returned signal ($Y(\omega)$) and the emitted signal ($X(\omega)$) (Eq. (1)), ω being the angular frequency [20]. $S_{11}(\omega)$ is measured at the connection between the antenna feed point and the vector network analyzer cable. The antenna can be modeled as a simple linear system composed of elementary model components which are included in the

resulting radar equation, expressed in the frequency domain as:

$$S_{11}(\omega) = \frac{Y(\omega)}{X(\omega)} = H_i(\omega) + \frac{H(\omega) \cdot G_{xx}^1(\omega)}{1 - H_f(\omega) \cdot G_{xx}^1(\omega)} \quad (1)$$

where $H_i(\omega)$ represents the complex return loss transfer function of the antenna, $H(\omega) = H_t(\omega) \cdot H_r(\omega)$ is the transmitting-receiving transfer function, $G_{xx}^1(\omega)$ is the Green's function describing 3-D wave propagation in the air-subsurface system modeled as a planar multilayered medium and $H_f(\omega)$ is the feedback loss transfer function of the antenna. The analysis of this reflected signal enables the estimation of soil layer depths and different soil characteristics like water content using full-wave inverse modeling. The Lambot et al. approach was chosen for

this study. For a more detailed explanation about the electromagnetic model, the reader is referred to Lambot et al. [19,20].

In order to identify subsurface parameters, inverse modeling is applied. Inversion is a nonlinear optimization method which consists of finding a parameter vector \mathbf{b} so that an objective function $\Phi(\mathbf{b})$ is minimized [20,26]. This inverse method employed for this case study utilizes least squares. In particular, we applied the inversion scheme presented in Lambot et al. (2006) [7]. The objective function is described by the following equation:

$$\varphi(\mathbf{b}) = |G_{xx}^{\dagger*} - G_{xx}^{\dagger}|^T C^{-1} |G_{xx}^{\dagger*} - G_{xx}^{\dagger}| \quad (2)$$

where $G_{xx}^{\dagger*} = G_{xx}^{\dagger*}(\omega)$ contains the observed Green's function, whereas $G_{xx}^{\dagger} = G_{xx}^{\dagger}(\omega, \mathbf{b})$ contains the simulated Green's function for a set of parameters [21]. $\mathbf{b} = [\varepsilon_r, h]$, in our case with ε_r being the relative dielectric permittivity (dimensionless) and h (m) being the antenna height above the ground (i.e., the distance between the medium and the antenna phase centre).

As our objective function only contains two parameters to be optimized, we resorted to a look up table (LUT) approach to find its minimum. Hence, for each radar measurement, the objective function was calculated in the full parameter space and its minimum was therefore directly found. Resorting to a LUT in this case was much faster than using an optimization algorithm and the found parameters always represent the global minimum of the objective function. Fig. 3 shows an example of objective function as obtained in this study. We can observe that the global minimum of the objective function is well defined. The soil moisture was then derived from the relative permittivity using Topp's model [22]. As we are only interested in the spatial distribution of soil moisture and not directly in its absolute value, we did not perform any site-specific calibration. Given the nature of the soil surface, i.e., sand, the expected error is less than 3% in terms of absolute soil moisture (e.g., see Lambot et al. (2004) [19]).

Topp's equation (Equation (3)) describes the relationship between soil moisture and relative dielectric permittivity:

$$\theta_v = -0.053 + 0.0293\varepsilon_r - 0.00055\varepsilon_r^2 + 0.0000043\varepsilon_r^3 \quad (3)$$

where θ_v is the volumetric soil water content (dimensionless) and ε_r is the relative dielectric permittivity (dimensionless).

Full-waveform inversion was focused on the surface reflection only [7,21], which for the frequency range employed in this study (560–700 MHz) provides soil moisture values mainly characterizing the top 5–10

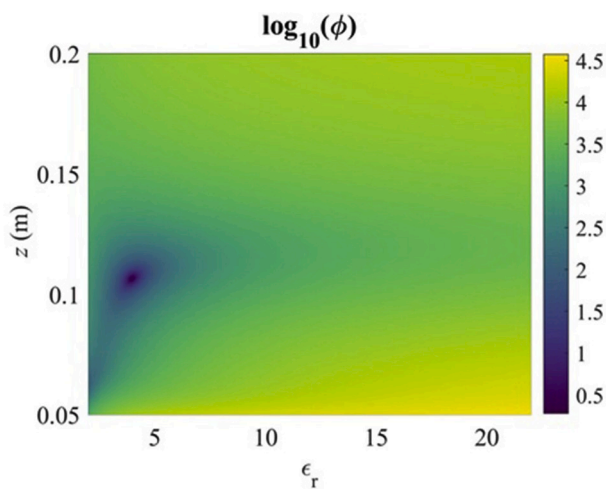


Fig. 3. Example of objective function to retrieve both the antenna height h and the relative permittivity ε_r from the radar measurements using full-wave inversion. (Color should be used). (For interpretation of the references to color in this figure legend, the reader is referred to the Web version of this article.)

cm of soil. In fact, according to Lambot et al., the characterized depth for a frequency range of 100–900 MHz, is slightly greater than 8 cm. For a more detailed explanation about the characterized depth, the reader is referred to Lambot et al. [7].

- Soil-surface moisture mapping

To cover a significant portion of the forest stand, we gathered 14 GPR transects (Fig. 4). Each transect is composed of about 2500 measurements and positioned by interpolation with geographical coordinates. Transects are located between two rows of trees and two transects are separated by three rows of trees (distance of about 9 m between each transect). Therefore, 42 rows of cork oak trees were covered by the radar measurements. Without access to a perfect electrical conductor (such as a large copper plate) to carry out the antenna calibration *in situ*, we executed a calibration on top of a daya (temporary pond) that was located near our forest stand. This calibration enabled us to determine the antenna transfer functions and thereby to filter out antenna effects during post-processing of the raw data, namely, to calculate the Green's functions from our S11 measurements. The permittivity of the water was calculated using Debye's model [23] combined with the model of Klein and Swift [24] to account for temperature (see Refs. [25]). The pond was assumed as a half-space medium as no reflection from the bottom of the pond was observed in the radar data. In addition to these radar transects, free-space measurements were taken before each transect to correct the H_i specific of each radar transect to account for possible radar drifts. Note that data from the first transect were not considered in our analyses as they were apparently subject to a significant and systematic over-estimation of the soil moisture values. This may be linked to the fact that the GPR had no yet reached a constant functioning temperature.

Using the inversion method explained previously, the relative dielectric permittivity ε_r was first estimated for each GPR data acquisition point. Then, using the kriging method on ArcGIS program, dielectric permittivity of neighboring points was estimated by interpolation. The ordinary kriging method was chosen and the searching neighborhood was specified (25 neighbors including at least 5 points). An exponential semi-variogram model was chosen with no anisotropy. Using the same kriging method previously described, the volumetric soil surface water content was then mapped based on Topp's equation. Then, using ArcGIS tools, the mean surface soil volumetric water content (θ_v) per dendrometric plot was estimated. For each plot, every θ_v point included in a dendrometric plot was selected and a mean value was then calculated. Note that there are no measured values for plots 1 and 8 considering that no GPR data points crossed these plots. Moreover, values recorded for plots 4, 10, 15, 22 and 34 were not included either as we believe that the first transect may have been subject to significant errors as explained above. The remaining mean values per plot were used in further analyses to link soil surface moisture to other variables such as tree growth and clay layer depths.

2.2.2. Time-domain radar system for subsurface structures imaging

In order to image the subsurface structures such as textural transitions (i.e., sand and clay layers), we used a time domain radar (SIR-20, Geophysical Survey Systems, Inc., Salem, Massachusetts, USA). Measurements were acquired in December 2015 by Dr. Frédéric André (UCLouvain, ELI-E). We used a 400 MHz centre-frequency antenna to reach at least 2.5 m depth. Positioning of the transects was done using a dGPS and positioning along the transects was done using the survey wheel of the radar system. Measurements were acquired every 2 cm along the transects.

To convert the wave propagation time (t) of the y-axis of the radar images into depth (z), the following equation was applied:

$$z = \frac{t}{2} \frac{c}{\sqrt{\varepsilon_r}} \quad (4)$$

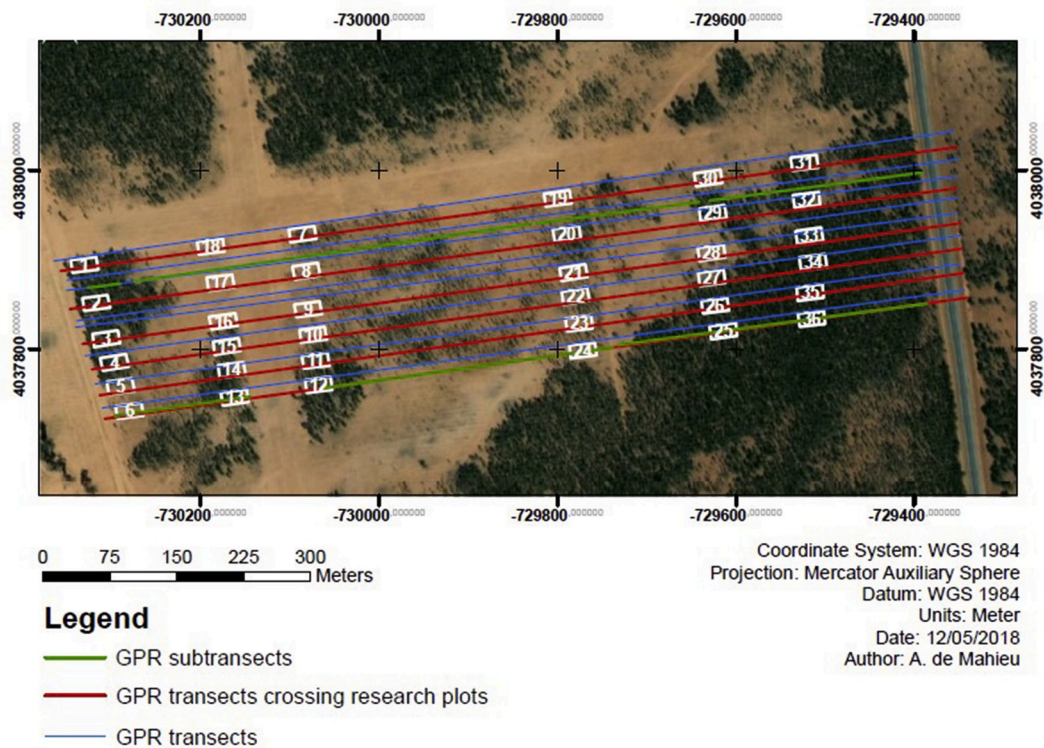


Fig. 4. Location of the 14 frequency-domain GPR transects (red: across dendrometric plots; blue: outside dendrometric plots), the 7 time-domain GPR subtransects (green) and the 36 dendrometric plots over a satellite view of the study stand. (Color should be used). (For interpretation of the references to color in this figure legend, the reader is referred to the Web version of this article.)

where z is the depth [m], t the wave propagation time [s], c the wave speed in free space ($c = 3.10^8$ m/s) and $\epsilon_r = 5$ (which corresponds to a slightly humid sand). In addition, the first reflection, which corresponds to the soil surface, was positioned at $z = 0$ m (offset of 0.75 m). Hence, the time-domain radar images allowed us to estimate the textural transition depths.

In our case, two main transects crossed the forest stand and were divided into seven sub-transects (2A, 2B, 1, 2, 3, 4 & 5) (Fig. 4). For each dendrometric plot crossed by one of the seven sub-transects, the depth of the textural transition measured by the radar was estimated. Note that we do not have information on the textural transition depths of plots 1 and 36.

2.3. Tree and soil surveys

2.3.1. Tree surveys

Based on a preliminary GPR signal map and the GeoEye satellite image of the study area, 36 rectangular 288 m² plots (12 m × 24 m, each including 32 potential tree locations) were installed to capture the full range of soil properties and tree characteristics (Fig. 4). They are crossed by six out of fourteen GPR transects (red colored transects in Fig. 4).

The plots were referenced by four markers on each corner and GPS coordinates were measured with a handheld *Trimble Juno 3D* GPS system. Within each plot, the circumference (C) and total height (H) of all trees were measured. Additionally, dominant height (H_{dom}), basal area (BA) and survival rate (S_r) were calculated based on the field measurements. The survival rate equals to the number of living trees divided by the sum of standing living and dead trees, tree stumps and empty locations expressed in percentage.

2.3.2. Soil surveys

Soil surveys were carried out systematically on each plot crossing a GPR transect using a 2-m long soil auger. Geographical coordinates of

each survey were taken using the same *Trimble Juno 3D* GPS in order to associate them with the GPR data. Soil cores of 0.2 m long were extracted from the ground and laid down in order to reassemble the soil horizons. Pictures were taken, observations were made and 3 to 6 samples from different horizons were collected for further analyses. The pictures and observations of the reassembled profiles allowed us to determine the sand types (based on their color) and to characterize the clay horizons in terms of consistence and reduction/oxidation processes.

Soil texture was first estimated for all 0.2 m cores from the 36 soil profiles using a “hand-touch sensation method” [27]. Then, soil texture was determined on selected 0.2 m cores for 16 out of 36 profiles by performing sieve analyses: the densimeter method was applied for 13 soil profiles at the National Institute of Agricultural Research of Rabat (INRA, Rabat) and the pipette method was carried out for 3 other soil profiles the UCLouvain soil laboratory (UCLouvain, Louvain-la-Neuve).

2.4. Qualitative and quantitative relationships between local site properties and tree performance

As a first step, we compared the soil moisture with the vigor of the cork oaks using the generated soil surface map and the satellite view (GeoEye satellite) of the forest stand. We also analyzed the reassembled soil profiles to determine the sand types (according to soil color) and clay consistence and estimated the soil texture using the hand-touch sensation method and then compared it to the soil moisture map.

As a second step, we studied the linear relationships between the main variables of our study. These are: the dominant heights H_{dom} which indicate the tree performances, the volumetric soil surface water contents θ_v given by the frequency-domain GPR, the clay content at 2 m of depth measured by the sieve analyses and the textural transition depths z indicated by the time-domain GPR. Simple linear regression models were applied using the *Matlab* software.

3. Results

3.1. GPR-derived surface soil moisture map

Fig. 5 shows the surface [0–10 cm] soil moisture map of our study area obtained by kriging using the frequency domain GPR. It is based on the 13 GPR transects (without the first transect) that were drawn with the radar system (Fig. 4). The volumetric water content θ_v varies between $0.013 \text{ m}^3/\text{m}^3$ (brown color which illustrates drier areas) and $0.1069 \text{ m}^3/\text{m}^3$ (blue color which represents more moist areas). When comparing this map to the satellite view of the forest stand (Fig. 4), we can distinguish that trees are much more vigorous where θ_v is higher. For example, this is observable in the lower right corner of this map.

3.2. Subsurface radar image

The radar images obtained with the commercial time domain GPR allowed us to estimate the textural transition depths between the sand and clay layers of the 7 sub-transects (Fig. 4). The estimated depths for the 10 dendrometric plots crossed by one of the seven sub-transects vary between 1.8 m and 4.2 m. Plot 19 is characterized by the deepest textural transition depth (4.2 m) while plots 12 and 30 have the shallowest depths (1.8 m). These textural transition depths can vary significantly on short distances. To illustrate, plots 12 and 13 are distant of about 50 m and the transition depths vary from 1.8 m to 3.0 m. Moreover, plots 30 and 31 which are also distant of about 50 m have transition depths that vary between 1.8 m and 2.5 m.

Fig. 6 shows an example of an image of the time-domain radar. It corresponds to sub-transect 4 (Fig. 4). The surface reflection is distinguishable on the top of the radar image by a bright blue-yellow colored stripe (at $z = 0 \text{ m}$). At a depth $z \approx 3 \text{ m}$, important reflections are observable along the sub-transect. These are due to a change in soil electromagnetic properties most likely originating from a textural

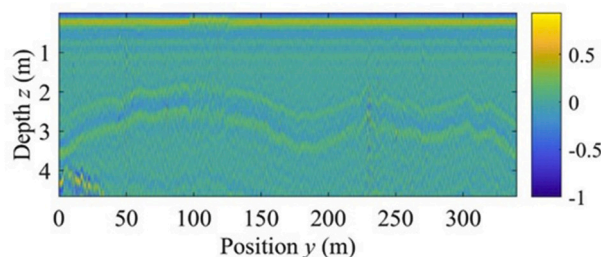


Fig. 6. Subsurface radar image of sub-transect 4 using a time domain commercial GPR (central frequency = 400 MHz) (André, 2015). The color scale represents the normalized signal amplitude (dimensionless). (Color should be used). (For interpretation of the references to color in this figure legend, the reader is referred to the Web version of this article.)

transition or waterfront. However, we cannot say with certainty that this continuous wave reflection indicates the clayey layer. This will be discussed later.

3.3. Performance of cork oaks

Table 1 shows the basic statistics related to tree measurements which are average tree circumference (C_{plot}), average height (H_{plot}), dominant height (H_{dom}), basal area (BA) and survival rate (S_r) per plot.

There is a high variability in terms of average circumferences, average heights and survival rates. Average circumference per plot varies between 16 cm and 60 cm and average height per plot between 2.2 m and 8.9 m. One third of the study plots have survival rates below 50%. Plots characterized by the lowest survival rates also have the lowest dominant heights. In addition, all these variables are strongly correlated. For example, the regression between C_{plot} and H_{plot} indicated a $R^2 = 0.96$ (p-value < 0.05). Hence, H_{dom} will be used as an integrated

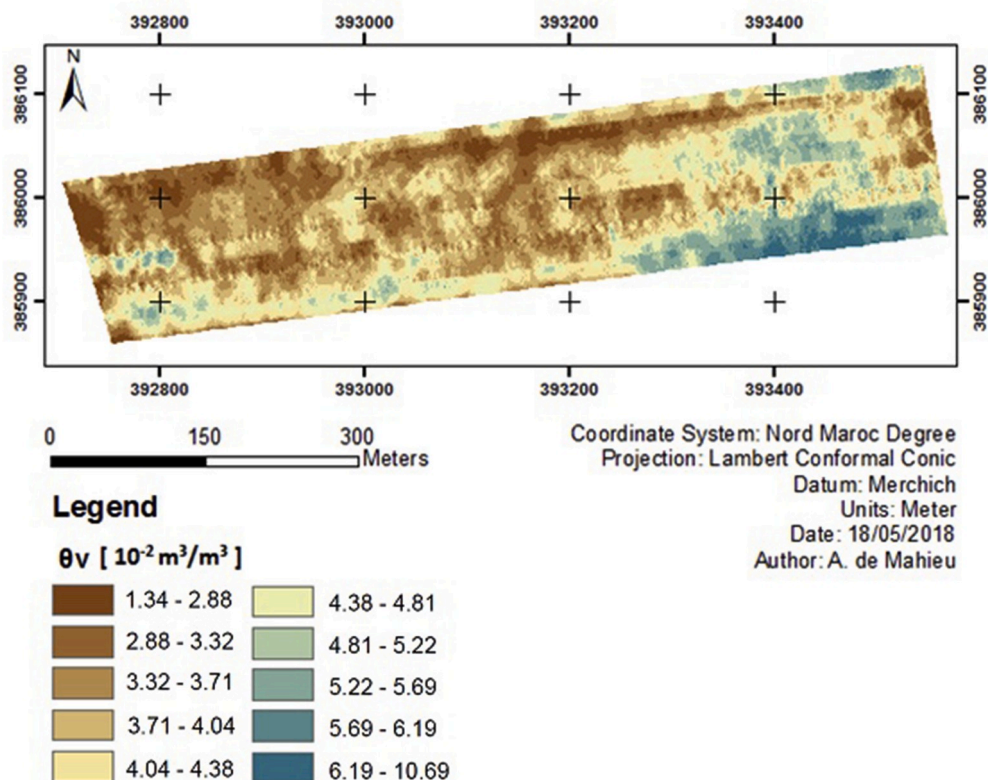


Fig. 5. Surface soil volumetric water content θ_v map of the study area obtained by kriging using the frequency domain GPR. (Color should be used). (For interpretation of the references to color in this figure legend, the reader is referred to the Web version of this article.)

Table 1

Basic statistics of the dendrometric variables per plot (mean, minimum (min), maximum (max), median, variance (var) and standard deviation (std)).

	Mean	Min	Max	Median	Var	Std
C_{plot} [cm]	35.8	16.0	60.3	34.6	117.9	10.9
H_{plot} [m]	5.0	2.2	8.9	4.5	3.3	1.8
H_{dom} [m]	6.3	2.2	10.2	5.9	5.0	2.2
BA [m ² /ha]	9.5	0.1	34.8	7.6	59.4	7.7
S_r [%]	58.2	5.6	100.0	61.8	651.3	25.5

performance measurement in the following analyses.

3.4. Soil layers characterization

3.4.1. Texture

Laboratory sieve analyses results for three soil profiles are depicted in Table 2. These three profiles characterize the different soil textures that were found throughout our forest stand according to the USDA soil texture diagram [28]: fine sand, loamy fine sand and sandy loam.

Generally, the surface soil horizons are mostly characterized by fine sand textures. Clay contents are very low and never exceed 5%. Silt contents are quite low as well in the majority of these horizons, but the percentages increase in some profiles. When summing up clay and silt contents of these profiles, we obtain high contents of fine elements (>15%). These surface horizons are characterized as loamy fine sands. Hence, above 150 cm of depth, sand prevails with contents exceeding 85%. However, in deep soil horizons (150–200 cm), the clay contents increase in a significant way (10–22%). These soil horizons are hence characterized by sandy loam (or sandy clay loam) textures. In contrast, clay contents in some profiles do not exceed 5%, even in deep soil layers (>200 cm). Thus, the textural transition is deeper in these soil horizons.

Soils of our study plots are hence composed of a sandy layer on top of a sandy-clay layer. The transition between the sand and clay layers can be abrupt or progressive by means of a sandy-clay layer frequently ochre-colored and where traces of hydromorphy can be found (e.g., ferruginous concretions and rust colored spots).

3.4.2. Sand types

Three types of sands are found in Maãmora soils: beige-pink sands, red sands and white-grey sands. When all three types are found on the same profile, they overlap in the order presented. According to Lepoutre, beige-pink sands and white-grey sands are essentially siliceous and do not contain fine elements of a size lower than 20 µm. In contrast, red sands can contain up to 15–18% of fine elements such as clay [4]. In some soil profiles, hydromorphic traces are observable in the sands overlaying the clay layer: white and red spots, ferruginous concretions etc. All three sand types are found in our study area. Red sands are mostly found in the eastern part of the stand where trees are bigger and where the top-soil is moister while the beige sands are found in the central and western parts of the stand.

Table 2

Laboratory sieve analyses of three soil profiles: n° 7, 16 and 32. Soil textures are determined using the pipette method (UCLouvain) for profile 7 and using the densimeter method (INRA) for profiles 16 and 32.

Plot	Depth [cm]	Clay [%]	Silt [%]	Sand [%]	Texture
7	0–20	3.30	2.45	94.25	Fine sand
	100–120	1.81	2.06	96.13	Fine sand
	180–200	5.65	3.92	90.43	Fine sand
	200–220	7.12	4.94	87.94	Loamy fine sand
16	0–20	2.48	3.73	93.79	Fine sand
	140–160	2.41	3.62	93.97	Fine sand
	200–220	2.38	9.52	88.10	Fine sand
32	0–20	2.33	13.98	83.69	Loamy fine sand
	100–120	2.32	10.45	87.23	Fine sand
	160–180	15.75	20.25	64.00	Sandy loam

3.4.3. Clay horizons

Clay color and consistence vary from one soil profile to another. As mentioned above, clay horizons are found beneath the sandy layers at a depth starting at approximately 1.80 m. Two types of clay were found on our study plot: grey moist sticky clays and dry friable red clays. The grey clays were mostly observed in the western part of the study plot while the red clays were located in the eastern part where the trees are more vigorous.

3.5. Regression models between soil and tree properties

Finally, this subsection presents the linear relationships between the main variables of our study.

3.5.1. Tree growth and soil surface moisture

We previously observed on the map of our study area (Fig. 5) that the mean surface soil volumetric water content seemed to be higher in areas where trees were bigger and more vigorous. This is confirmed by the linear and positive relationship between dominant height and mean θ_v per plot (Fig. 7). Nevertheless, it is interesting to note that some plots depart from this general trend. For example, plot 31 has a high dominant height ($H_{dom} > 9$ m) but its water content is relatively low ($\theta_v < 0.035$) whereas plot 17 has a high water content ($\theta_v > 0.05$) but a low dominant height ($H_{dom} < 3$ m).

3.5.2. Soil surface moisture and soil texture

We then crossed the mean surface soil volumetric water content (θ_v) and the clay content in deep horizons ($z \approx 2$ m). As shown in Fig. 8, we observe a positive linear relationship between both variables. Plots 26 and 29 have relatively high clay contents beyond 1.5 m of depth (>18%) and high soil moisture ($\theta_v > 0.045$). Moreover, they both have a successful tree growth characterized by high trees ($H_{dom} > 7$ m, see Fig. 7). In contrast, clay contents in depth ($z \approx 2$ m) are very low for plot 19 (<3%); this profile has a fine sand texture and low soil moisture ($\theta_v < 0.025$). This plot is also characterized by a low dominant height ($H_{dom} < 4$ m, see Fig. 7).

3.5.3. Tree growth and soil texture

As dominant height has a positive linear relationship with surface water content (Fig. 7) and surface water content has also a positive linear relationship with clay content in depth (Fig. 8), we assumed that the dominant height would be related to clay content in depth as well. This is illustrated in Fig. 9 which shows the dominant height per plot as a

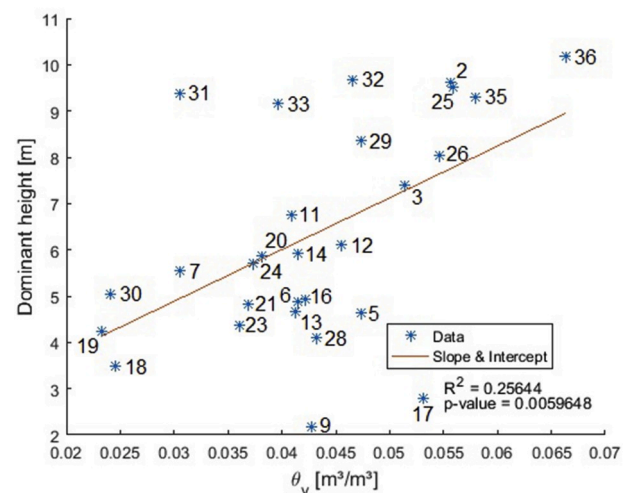


Fig. 7. Dominant height (H_{dom}) as a function of the mean surface soil volumetric water content (θ_v) with linear regression. Data points (*) are marked by their respective plot number.

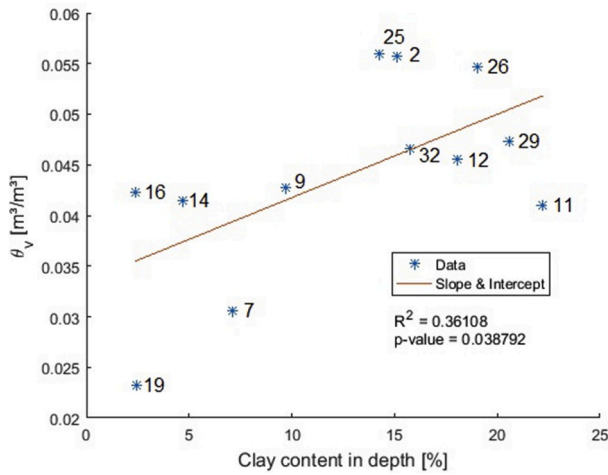


Fig. 8. Mean surface soil volumetric water content (θ_v), as a function of the clay content at a depth of about 2 m with linear regression. Data points (*) are marked by their respective plot number.

function of the clay content in depth ($z \approx 2$ m).

As expected, a positive linear relationship is observed between both variables. For example, plots 26 and 29 are characterized by high dominant heights ($H_{dom} > 7$ m) and high clay contents in depth ($> 18\%$). In contrast, plots 16 and 19 have lower dominant heights ($H_{dom} < 5$ m) which might be explained by the low clay contents in depth ($< 5\%$). Once more, some exceptions are observable such as plot 9 which is characterized by a very low dominant height ($H_{dom} < 3$ m) but an average clay content.

3.5.4. Clay layer depth

Finally, based on the six soil profiles where both time domain GPR and texture data were available, we obtained Fig. 10 which shows the textural transition depth estimated per plot using the 2015 radar images as a function of the clay content in depth per plot ($z \approx 2$ m). For each plot crossed by one of the seven sub-transects, the depth of the textural transition measured by the radar is plotted in the vertical axis. Although the number of points is limited, a full range of clay contents is observed and thus, represents the variation observed in our study area.

As the textural transition depth decreases, the clay content in depth increases. Plots 12 and 29 have both high clay contents in depth (18%

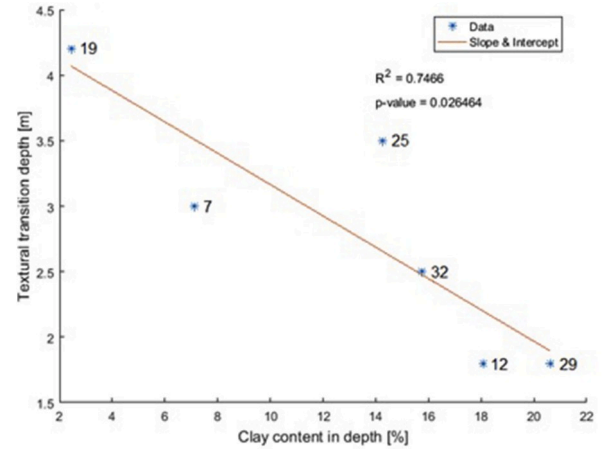


Fig. 10. Textural transition depth as a function of the clay content at a depth of about 2 m with linear regression. Data points (*) are marked by their respective plot number.

and 21%). The radar image confirms that there is a textural transition at approximately the same depth (1.8 m). When the clay content at 2 m depth decreases down to 2% (plot 19), the textural transition depth measured by the radar is much deeper (4.2 m). The low clay content indicates that the sand layer is thicker in this profile than in plots 12 and 29. The relationship between these variables confirms the compliance of the 2015 radar data with our soil laboratory results.

3.6. Discussion

Our first objective was to test the relevance of using both frequency and time-domain GPR to characterize the small-scale spatial variability of the soil physical properties. According to the surface soil moisture map (Fig. 5) obtained using the frequency-domain GPR, we observed that the volumetric water content could vary significantly over short distances. In view of Fig. 8, soil texture seemed to be the main factor determining soil water content variation. Compared to the θ_v in a saturated sandy soil ($\theta_{v,sat} \approx 0.4 \text{ m}^3/\text{m}^3$) [29], the measured values represent more or less one quarter of the possible humidity variation, suggesting our θ_v were probably underestimated. As explained above, the characterized depth for the employed frequency range of the GPR is slightly greater than 8 cm [7]. Although the top first centimeters of sand appeared to be indeed dry during the field campaign, the lower layers looked relatively moist. As a result, either our characterization depth was lower than expected, the dry-moist dielectric contrast led to interferences, or the obtained values were underestimated. Nevertheless, the map presented in Fig. 5 is especially useful to highlight soil relative moisture patterns within the field. The values of mean θ_v per plot are hence compared from one plot to another and not in absolute value, so any bias of θ_v is not expected to impact data interpretation.

Using the commercial time-domain GPR, we were able to estimate soil textural transition depths (Fig. 6). These presumed textural transitions were detected by radar reflections (variation in color on Fig. 6). The reflection at an interface is in fact characterized by an oscillation between a positive maximum and a negative minimum. The presence or absence of water in the material is the principal factor determining the soil electrical conductivity and dielectric permittivity. However, other soil variables can affect the electromagnetic properties such as soil texture (mainly clay content), structure, soluble salts, temperature and density [8]. The sand, silt and clay contents in depth measured by the sieve analyses provided complementary information as abrupt textural transitions were detected at similar depths to the radar reflections. We cannot say with certainty that the continuous wave reflection observed on the radar images indicate the clayey layers as such. In fact, other

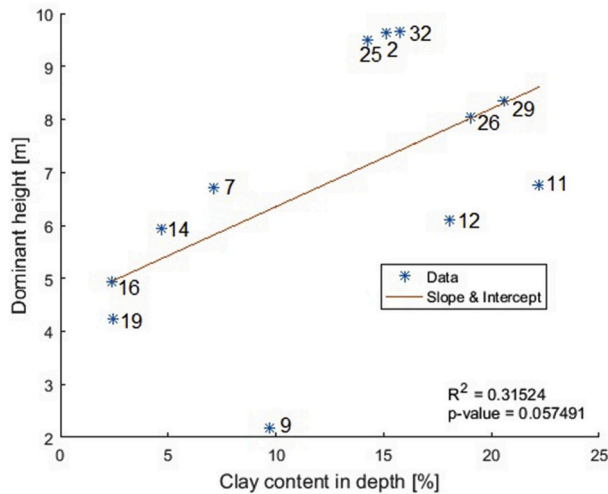


Fig. 9. Dominant height (H_{dom}) as a function of the clay content at a depth of about 2 m with linear regression. Data points (*) are marked by their respective plot number.

important reflections are sometimes observable beneath the main reflection. This means that the electromagnetic (EM) waves were not completely attenuated within this second layer and thus its clay content is expected to remain relatively low. We assume that this reflection is rather a textural transition than a contrasted waterfront for the same reason, as EM waves would have been much more attenuated if this second layer had been very moist. Nevertheless, textural transitions are usually associated to moisture transitions due to the varying water retention curves as a function of texture. In fact, hydromorphic stains were detected in some deep horizons characterized by rust stains and moist pseudogley.

Both radar systems hence provided information on soil properties and in particular on their spatial distribution. The frequency-domain GPR provided information on soil moisture (lateral distribution) and the commercial GPR on textural transition depths (vertical distribution).

Our second objective was to link the previously identified soil physical properties to plant response. In view of Fig. 7, soil water content, which is influenced by soil texture (see Fig. 8), inextricably affect tree performance. Given the same atmospheric boundary conditions, a wetter soil denotes a higher overall soil water retention, which is a crucial factor for tree establishment and subsequent growth in arid or semi-arid environments [3]. Yet, there is an important residual variability when observing Fig. 7. The potential factors that are responsible of this variability are discussed.

First, the clay layer depth, estimated by the commercial time-domain GPR and the hydromorphic stains identified in the soil cores, is a factor that may explain the variability between soil moisture and tree performance. In fact, we assumed that when the clay content at 2 m depth is higher, the clay layer must be shallower than in profiles where the clay content is lower at the same depth. When a soil is humid (wet season), the surface horizons provide more water to the shallow tree roots than deep horizons. Then, when the soil starts to dry up (dry season), water extraction by tree roots will gradually occur deeper and deeper as less water is retained in the soil profile. In summer, only the deep tap roots will take up water. Hence, water uptake by tree roots occurs in different soil horizons according to the season [5]. As clays retain water more efficiently than sands which drain water more rapidly, the plots that contain more clay at 2 m depth must have better water retention. To confirm our assumptions, we observed once again in Fig. 9 a positive linear relationship between dominant height and clay content at 2 m of depth. The use of the radar images provided by the commercial GPR was complementary to the other GPR as it detected the higher contents of clay in the soil profile (textural transitions).

The clay consistence (and pseudogley) identified in depth also proved that our study plot may be subject to the effect of temporary waterlogging conditions (i.e., temporary perched water tables) which is unfavorable to many tree species [30], including the very sensitive cork oak [5]. The formation of a perched water table on top of the clay horizon occurs in winter (high precipitations) in areas where the sand cover is not too thick and where the slope is not too important [4]. This is the case on our study area as the slope is almost nil and the concerned soil profiles have an estimated textural transition depth below 2 m. This water table can lead to adverse effects on young seedlings as it can create anaerobic conditions and asphyxiate tree roots [31]. This occurs when the perched water table is very shallow. Moreover, if the young roots stop growing at the water table level, during the next summer, the roots not having reached the clay layer will dry up. When this water table disappears in summer, the soil is exposed to oxygen, and iron is oxidized. This is observable by red, yellow and orange stains in the upper soil horizons.

Another determining factor may be the different sand types observed in the first soil horizons. As explained above, three types of sands are found in Maãmora soils. The red sands – which are found in the eastern parts of the stand – better retain water than beige sands which are characterized by a higher permeability and a smaller water retention (see Fig. 5). The enrichment in clay in the red sandy profiles, and thus

the presence of fine elements ($\phi < 50 \mu\text{m}$) influence water retention. In fact, the soil ability to retain water is strongly related to particle size: fine particles of a clay lead to a finer porosity which holds more strongly water compared to a coarse sand [32]. Increased water retention in these areas can thus lead to a localized successful regeneration of seedlings as their roots have better access to water.

Besides soil factors, other factors including anthropic pressure can reinforce tree mortality. Shepherds let their animals graze which feed on acorns, small bushes and young tree seedlings when the vegetation is scarce. They sometimes feed on leaves and branches, cut down by their owners. Additionally, local inhabitants fell trees to sell the firewood to local markets. Human pressure is certainly not the main factor that affects successful regeneration of cork oak stands, but it can exacerbate tree mortality. Still, it is important to mention it as Maãmora forest has been subject to this issue for many years. Even though their actions are sensible in that socio-economical context, it pressures the forest and an appropriate balance must be found between different interests in order to ensure sustainability. In contrast, although climate is more or less identical throughout the distribution area of the cork oak species in the Maãmora forest, its impact can be more significant for trees that do not have access to appropriate soil water resources. Even though cork oaks are located in their most southern natural distribution area of the Mediterranean region, this species can survive in its natural habitat thanks to its capacity to resist to dry summers, when soil water deficits and high temperatures constrain the cork oak growth [33]. However, climate change characterized by warmer temperatures, lower precipitations and more frequent droughts could lead to higher mortality in the future.

4. Conclusion and perspectives

The overall aim of this research was to develop a method using GPR to characterize spatial variability of soil physical properties that can potentially affect the successful regeneration of cork oaks in a context of more or less deep sandy soils. To reach this aim, we proceeded in a geophysical characterization of the study area using GPR antennas, then linked the geophysical response with the soil physical properties and finally linked these properties to the tree responses. This was achieved by analyzing numerous field measurements. First, dendrometric measurements related to cork oak growth confirmed our observations on the high variability that prevails in our study area. Then, using our light-weight frequency domain GPR, the volumetric soil water content was measured and hence, we were able to map the soil surface moisture of the study area. Using past historic time domain GPR data, we were also able to detect at which depths the textural transitions between sandy and clay layers occur which are specific to the Maãmora soil profiles. Finally, soil surveys down to 2 m depth provided information on the sandy and clayey layers through laboratory analyses.

Throughout this study, both radar systems provided complementary information on soil properties and in particular on their spatial distribution. They allowed us to analyze their impact on cork oak growth. These properties are soil moisture and textural transition depth. Hence, we were able to detect soil factors that influence tree regeneration using a near-surface remote sensing tool which is GPR. Obviously, further soil analyses would allow us to fully understand the soil water hydrodynamics. In addition, studying the cork oak fine root system would help elucidate where and how water is extracted from the different soil horizons. Although we were not able to fully unravel all the factors that contribute to successful cork oak regeneration, nonetheless, GPR provided us with valuable information in an efficient manner with minimum operational requirement.

Using GPR for future cork oak planting would allow foresters (or private forest managers) to detect the best areas where trees should be planted in order to have a successful regeneration. Given the multiple factors determining tree vigor, future research could benefit of using machine learning approaches to predict the most suitable areas for tree

planting. GPR could in this way become a decision-support tool that would give valuable recommendations in terms of tree plantation in variable edaphic contexts but especially under constraining conditions such as coarse-textured soils under (semi-)arid climates.

Declaration of competing interest

None.

Acknowledgements

The authors would like to acknowledge the Wallonie-Bruxelles International administration which allowed the implementation of this project which falls within bilateral cooperation between the Ecole Nationale Forestière d'Ingénieurs de Salé (ENFI, Morocco) and the Earth and Life Institute of the Université catholique de Louvain (UCLouvain, Belgium). The authors are also grateful to the Fonds de la Recherche Scientifique (FNRS) which funded the GPR-related research.

We would also like to express our profound gratitude to Mr. Brahim Ahsissou and Mr. Arbi Elhakour, driver and technician of ENFI, respectively, for their help, enthusiasm and good spirit in the field. We are grateful to Mrs. Anne Iserentant, laboratory assistant at UCLouvain, as well as to Mr. Saïd Harati and Mr. Hafid Chafori, soil technicians of the National Institute of Agricultural Research of Rabat (INRA), for their assistance in processing the soil analyses. Finally, we would also like to thank Mr. Frédéric Laurent, UCLouvain technician for building the horn dipole antenna of the frequency-domain GPR as well as Dr. Frédéric André, UCLouvain scientific researcher who took the commercial GPR measurements back in 2015. The final version of the manuscript benefited from the wise advice of three anonymous reviewers.

References

- [1] Salem BB. Forest resources division, FAO. *Arid zone forestry: a guide for field technicians*, vol. 20; 1989. p. 143. FAO Conservation Guide.
- [2] Food and Agriculture Organization of the United Nations. *State of the world's forests, Forests and Agriculture: land-use challenges and opportunities*. 2016. p. 126. Rome.
- [3] Malagnoux M. *Arid land forests of the world: global environmental perspectives*. Forestry Department FAO; 2007. p. 14.
- [4] Lepoutre B. *Régénération artificielle du chêne-liège et équilibre climacique de la subéraie en forêt de la Maâmora*, vol. 9. *Annales de la recherche forestière au Maroc*; 1965. p. 185. Rapport annuel, Tome.
- [5] Aronson J, Pereira JS, Pausas JG. Cork oak woodlands on the edge: ecology, adaptive management, and restoration. *Society for Ecological Restoration International*; 2009. p. 352.
- [6] Food and Agriculture Organization of the United Nations. *Global guidelines for the restoration of degraded forests and landscapes in drylands. Building resilience and benefiting livelihoods*, vol. 175. Rome: FAO Forestry Paper; 2015. p. 148.
- [7] Lambot S, Weihermüller L, Huisman JA, Vereecken H, Vanclooster M, Slob EC. Analysis of air-launched ground-penetrating radar techniques to measure the soil surface water content. *Water Resour Res* 2006;42:12. <https://doi.org/10.1029/2006WR005097>. W11403.
- [8] Jol HM. *Ground-penetrating radar: theory and applications*. Amsterdam: Elsevier Science; 2009. p. 508.
- [9] Laariby S, Gmira N, Alaoui A. Towards a coordinated development of the forest in Maâmora, Morocco. *J. For. Fac.* 2010;10(2):172–9. Kastamonu Univ.
- [10] Belghazi B, Mounir F. Optimiser la production de biens et services par les écosystèmes boisés méditerranéens dans un contexte de changements globaux, Analyse de vulnérabilité au changement climatique du couvert forestier, *Rapport technique*. FAO; 2016. p. 127.
- [11] Belghazi B, Badouzi M, Belghazi T, Moujjani S. Semis et plantations dans la forêt de chêne-liège de la Maâmora, Maroc, *Forêt méditerranéenne*, Tome 2011;3:301–14. 32.
- [12] Bagaram BM, Mounir F, Lahssini S, Ponette Q. Site suitability analysis for cork oak regeneration using GIS based multicriteria evaluation techniques in maamora forest-Morocco. *Open Access Libr J* 2016;3:9. <https://doi.org/10.4236/oalib.1102483>.
- [13] Noumonvi KD, Mounir F, Belghazi B. Spatial multi-criteria based analysis to assess dynamics and vulnerability of forest ecosystems to global changes: case of maamora forest-Morocco. *Open Access Libr J* 2017;4:16. <https://doi.org/10.4236/oalib.1103889>.
- [14] El Boukharri EM, Brhadda N, Gmira N. Bilan actualisé et facteurs impliqués dans le succès des reboisements du chêne-liège (*Quercus suber* L.) dans la forêt de la Maâmora, Maroc. *Geo-Eco-Trop* 2015;38(2):325–38.
- [15] Thornthwaite CW. An approach toward a rational classification of climate. *Geogr Rev* 1948;28(1):55–94. <https://doi.org/10.2307/210739>.
- [16] Climate Data. Salé, maroc. <https://fr.climate-data.org/afrrique/maroc-181/#example2>. [Accessed 14 May 2018].
- [17] Texier J-P, Lefèvre D, Raynal J-P. La formation de la Maâmora : le point sur la question du Moulouyen et du Salétien du Maroc Nord-Occidental. In: *Quartenaire*, vol. 3; 1992. p. 63–73. <https://doi.org/10.3406/quate.1992.1974.2>.
- [18] Himpens S. Impacts de la profondeur d'apparition de la couche d'argile sur le succès de reboisement en chêne-liège en forêt de Maâmora (Maroc). UCLouvain: *Mémoire de fin d'études*; 2016. p. 116.
- [19] Lambot S, Slob EC, van den Bosch I, Stoeckbroeckx B, Vanclooster M. Modeling of ground-penetrating radar for accurate characterization of subsurface electric properties. *IEEE Trans Geosci Rem Sens* 2004;42(11):2555–68. <https://doi.org/10.1109/TGRS.2004.834800>.
- [20] Lambot S, André F. Full-wave modeling of near-field radar data for planar layered media reconstruction. *IEEE Trans Geosci Rem Sens* 2014;52(5):2295–303. <https://doi.org/10.1109/TGRS.2013.2259243>.
- [21] Lambot S, Antoine M, van den Bosch I, Slob EC, Vanclooster M. Electromagnetic inversion of GPR signals and subsequent hydrodynamic inversion to estimate effective vadose zone hydraulic properties. *Vadose Zone J* 2004;3:1072–108. <https://doi.org/10.2113/3.4.1072>.
- [22] Topp GC, L Davis J, Annan AP. Electromagnetic determination of soil water content: measurements in coaxial transmission lines. *AN AGU J* 1980:574–82. <https://doi.org/10.1029/WR016i003p00574>.
- [23] Debye P. *Polar molecules*. Reinhold; 1929. p. 172.
- [24] Klein LA, Swift CT. An improved model for the dielectric constant of sea water at microwave frequencies. *IEEE Trans Antenn Propag* 1977;25(104–111):104–11. <https://doi.org/10.1109/TAP.1977.1141539>.
- [25] Tran AP, Ardekani MRM, Lambot S. Coupling of dielectric mixing models with full-wave ground-penetrating radar signal inversion for sandy-soil-moisture estimation. *Geophysics* 2012;77(3):H33–44. <https://doi.org/10.1190/geo2011-0100.1>.
- [26] Minet J, Bogaert P, Vanclooster M, Lambot S. Validation of ground penetrating radar full-waveform inversion for field scale soil moisture mapping. *J Hydrol* 2012; 424–425:112–23. <https://doi.org/10.1016/j.jhydrol.2011.12.034>.
- [27] Hassan BJ. *Protocole d'évaluation de la texture au toucher*. 1 page. Ecole nationale forestière d'ingénieurs de Salé; 1988.
- [28] United States Department of Agriculture (Usda). Soil texture calculator, NRCS soils. Natural resources conservation service soils. s.d, https://www.nrcs.usda.gov/wps/portal/nrcs/detail/national/soils/?cid=nrsc142p2_054167. [Accessed 15 April 2018].
- [29] Carsel RF, Parrish RS. Developing joint probability distributions of soil water retention characteristics. *Water Resour Res* 1988;24:755–69. <https://doi.org/10.1029/WR024i005p00755>.
- [30] Levy G, Lefèvre Y. *La forêt et sa culture sur sol à nappe temporaire : contraintes subies, choix des essences, interventions et gestion durable*. Nancy, FRA: ENGREF; 2001. p. 223.
- [31] Jabiol B, Lévy G, Bonneau M, Brêthes A. *Comprendre les sols pour mieux gérer les forêts : contraintes et fragilité des sols, choix des essences, précautions sylvicoles, améliorations*. Agro-Paris-Tech; 2009. p. 624.
- [32] Kirkham MB. *Principles of soil and plant water relations*, vol. XVII. Amsterdam: Elsevier; 2010. p. 500.
- [33] David TS, Henriques MO, Kurz-Besson C, Nunes J, Valente F, Vaz M, Pereira JS, Siegwolf R, Chaves MM, Gazarini LC, David JS. Water-use strategies in two co-occurring Mediterranean evergreen oaks: surviving the summer drought. *Tree Physiol* 2007;27:793–803.